Choroidal Vascular Fingerprints From Indocyanine Green Angiography Unveil Chorioretinal Disease State

Ruoyu Chen,[1] Ziwei Zhao,[1] Mayinuer Yusufu,[2,3] Xianwen Shang,[1] Mingguang He,[1,4,5] and Danli Shi[1,4]

[1]School of Optometry, The Hong Kong Polytechnic University, Kowloon, Hong Kong SAR, China
[2]Centre for Eye Research Australia, Royal Victorian Eye and Ear Hospital, East Melbourne, Australia
[3]Department of Surgery (Ophthalmology), The University of Melbourne, Melbourne, Australia
[4]Research Centre for SHARP Vision, The Hong Kong Polytechnic University, Kowloon, Hong Kong SAR, China
[5]Centre for Eye and Vision Research (CEVR), 17W Hong Kong Science Park, Hong Kong SAR, China

Correspondence: Danli Shi, School of Optometry, The Hong Kong Polytechnic University, Kowloon, Hong Kong SAR, China; danli.shi@polyu.edu.hk. Mingguang He, Experimental Ophthalmology, School of Optometry, The Hong Kong Polytechnic University, Kowloon, Hong Kong SAR, China; mingguang.he@polyu.edu.hk.

Received: August 23, 2024
Accepted: August 27, 2025
Published: October 1, 2025

Citation: Chen R, Zhao Z, Yusufu M, Shang X, He M, Shi D. Choroidal vascular fingerprints from indocyanine green angiography unveil chorioretinal disease state. *Invest Ophthalmol Vis Sci.* 2025;66(13):3. https://doi.org/10.1167/iovs.66.13.3

Purpose. To develop an annotation-efficient deep learning algorithm for extracting multidimensional features of choroidal vasculature on indocyanine green angiography (ICGA) images via a human-in-the-loop (HITL) strategy and explore their relationship with multiple chorioretinal diseases.

Methods. The segmentation model was trained on a multi-source dataset that included both 55° ICGA and 200° ultra-widefield ICGA (UWF-ICGA) images, using a HITL strategy. Choroidal vascular fingerprints were generated from the segmentation maps, quantifying diameter, density, complexity, tortuosity, and branching angle. Reliability was assessed using intraclass correlation coefficients (ICC), and normal ranges for each measurement were estimated. The study retrospectively included 243 eyes diagnosed with central serous chorioretinopathy (CSC), polypoidal choroidal vasculopathy (PCV), or pathological myopia (PM), as well as 151 normal control eyes, to investigate their association with choroidal vascular fingerprints. Multivariable logistic regression models were used for the analysis.

Results. The model achieved high segmentation accuracy, with the area under the receiver operating characteristic curve being 0.975 (95% confidence interval [CI, 0.967–0.983) for 55° view ICGA images and 0.937 (95% CI, 0.914–0.960) for UWF-ICGA images. Twenty-six, 28, and 29 multidimensional measurements were significantly associated with CSC, PCV, and PM, respectively (P value < 0.05). The ICC values for 74 choroidal vascular measurements ranged from 0.71 (95% CI, 0.51–0.84) to 0.97 (95% CI, 0.95–0.99).

Conclusions. This pioneering study revealed choroidal vascular fingerprints and validated their associations with various chorioretinal diseases. These findings pave the way for future exploration of the pathological mechanisms underlying these conditions.

Keywords: choroidal vessel segmentation, choroidal vascular measurement, indocyanine green angiography, imaging biomarker, human-in-the-loop strategy

The choroidal vascular network plays a vital role in delivering oxygen and nutrients to the outer retina. Abnormalities of choroidal circulation can induce progressive dysfunction of retinal pigment epithelium (RPE) and photoreceptors, which are increasingly recognized as critical contributors to the pathogenesis of various chorioretinal diseases.[1] Previous studies have established that pachychoroid spectrum diseases, such as central serous chorioretinopathy (CSC) and polypoidal choroidal vasculopathy (PCV), were associated with choroidal thickening and vascular morphological alterations.[2,3] Additionally, compromised choroidal perfusion has been correlated with choroidal thinning and myopia progression.[4,5] Quantification of these vascular changes may enhance our understanding of the pathological processes and inform targeted therapeutic strategies for chorioretinal pathologies.

Indocyanine green angiography (ICGA) remains the clinical gold standard examination for visualizing choroidal vasculature through contrast-enhanced imaging.[6] The advent of ultra-widefield ICGA (UWF-ICGA) technique further expanded diagnostic capabilities by enabling comprehensive evaluation of peripheral choroidal vasculature, including vortex vein morphology.[7] Several choroidal vascular characteristics observed on ICGA images have been extracted via manual segmentation or deep learning-based approaches for screening and monitoring chorioretinal conditions, such as vortex vein engorgement, fusiform choroidal vein, and vascular density in eyes with pachychoroidal diseases.[2,8–11] However, most of those studies relied on labor-intensive annotation, suffering from subjective interpretation and methodological variability. These drawbacks hinder both reproducibil-

ity and clinical translation. The development of automated systems for segmenting and quantifying multidimensional choroidal vascular features in ICGA and UWF-ICGA imaging remains unresolved in ophthalmic imaging research for establishing clinically robust choroidal biomarkers.

Despite advances in deep learning–based quantification of retinal vasculature in fundus imaging to precisely evaluate morphological alterations,[12,13] analogous progress in choroidal vascular analysis has been impeded by distinct anatomical and technical challenges. The complex structure of choroidal vascular plexus complicates vascular annotation and decreases the efficiency of model development. Recently, human-in-the-loop (HITL) strategies that integrate limited expert annotation with active learning frameworks have offered promising solutions for effective model training.[14,15] By integrating an interactive object detection architecture, this approach leverages clinician expertise to iteratively refine preliminary annotations generated by a pre-trained detector,[16,17] thereby avoiding a cold start of annotation within conventional model training. Collaboration between machine intelligence and human feedback could benefit both training efficiency and model performance.[18,19]

This study aims to develop an automated algorithm for segmenting choroidal vessels in ICGA and UWF-ICGA images and quantifying vascular features by integrating the deep learning framework with a HITL platform. This model is expected to achieve accurate measurements of choroidal vascular morphologies and provide multidimensional choroidal vascular fingerprints to enhance management of chorioretinal conditions.

Methods

We used deidentified existing data for our study, which received approval from the Institutional Review Board of the Hong Kong Polytechnic University.

Dataset

We used a multisource ICGA image dataset, comprising 55° view ICGA images and 200° view UWF-ICGA images, to develop this choroidal vessel segmentation model. The dataset includes ICGA images from patients with various chorioretinal diseases, including CSC, PCV, pathological myopia (PM), AMD, choroidal neovascularization, and ocular inflammatory diseases, as well as normal controls.

Because of the ineligibility of perfectly healthy individuals for invasive ICGA examinations, "normal controls" in this study were defined as patients who, although suspected of having choroidal vascular diseases and being recommended for ICGA examination, exhibited normal results on the ICGA results. All patient data underwent anonymization and deidentification. The 55° view ICGA and 200° view UWF-ICGA images were acquired using Heidelberg Spectralis cameras (Heidelberg Engineering, Heidelberg, Germany) and Optos Silverstone (Optos, Dunfermline, UK). To ensure precise segmentation of choroidal vascular network, we selected ICGA images captured between 30 seconds and three minutes after dye injection, because these early-phase images offer the clearest visualization of the choroidal vasculature.

Segmentation Model Development Using the HITL Strategy

Because no existing model is specifically designed for choroidal vessel segmentation in ICGA images, we leveraged a pretrained retinal vessel segmentation model as base model to generate pre-segmentation due to the tubular structural similarities between retinal and choroidal vessels.[20] The 55° view ICGA images were resized to 512 × 512 and fed into this pre-trained model. A threshold (ranging from 0 to 1) was used to binarize the vessel probability maps generated by the model. Specifically, the threshold was applied to convert continuous probability outputs into binary predictions to distinguish vascular from non-vascular regions. A human expert (D.S.) manually explored and adjusted the threshold to optimize the identification of visible choroidal vascular structures in ICGA images and reduce manual labeling efforts.

The interactive HITL strategy was used to fine-tune the pretrained model for choroidal vascular segmentation on ICGA images. Two experienced ophthalmologists (R.C and Z.Z) randomly selected 50 presegmented vessel maps for independent manual modification using a custom software (VesselLabel).[13] The presegmented choroidal vessel map could be overlaid on either the original ICGA images or the contrast-enhanced ones. The ophthalmologists could toggle between modes to correct vessel annotations suggested by the presegmentation model, including removing false labels (e.g., retinal vessels) and adding missing vessel annotations. Supplementary Figure S1 shows the interface of this custom vessel labeling software. A detailed protocol for human evaluation and modification is provided in Supplementary Figure S2. The Dice coefficient was used to assess the consistency between annotators.

In each HITL cycle, human-modified ICGA images (modified by R.C.) served as the ground truth and were randomly split into training, validation, and test sets in a ratio of 70%:15%:15%. Specifically, 70% of these modified vascular segmentations were used to fine-tune the model (training set), 15% were used to adjust hyperparameters and to select the best model configuration during the model development phase (validation set), and the remaining 15% were used as the final benchmark for assessing the model's performance on unseen data (test set).

Human-modified annotations in training set were used to fine-tune the pretrained model for 50 epoch. Next, we applied this refined model to new unlabeled ICGA images to generate predictions for the second version of choroidal vascular presegmentations, followed by further visual evaluation and corrections. This iterative process was integrated into the entire fine-tuning workflow and repeated until the model could segment the visible choroidal vessels in ICGA images. The training data from each cycle were cumulatively added to the training set of the previous cycle. To prevent data leakage, the test set for each cycle only included images that were newly labeled in that cycle and had never been used in any prior training or validation.

After the model achieved high accuracy in segmenting choroidal vascular in 55° view ICGA images, UWF-ICGA images were resized to 1024 × 1024 pixels and input into the model. The ophthalmologist (R.C.) randomly selected twenty UWF-ICGA pre-segmentations for modification, and a similar iterative cycle was repeated until the model successfully segmented visible vessels in the UWF-ICGA images. The flowchart of this study is shown in Figure 1A. The models

Investigative Ophthalmology & Visual Science

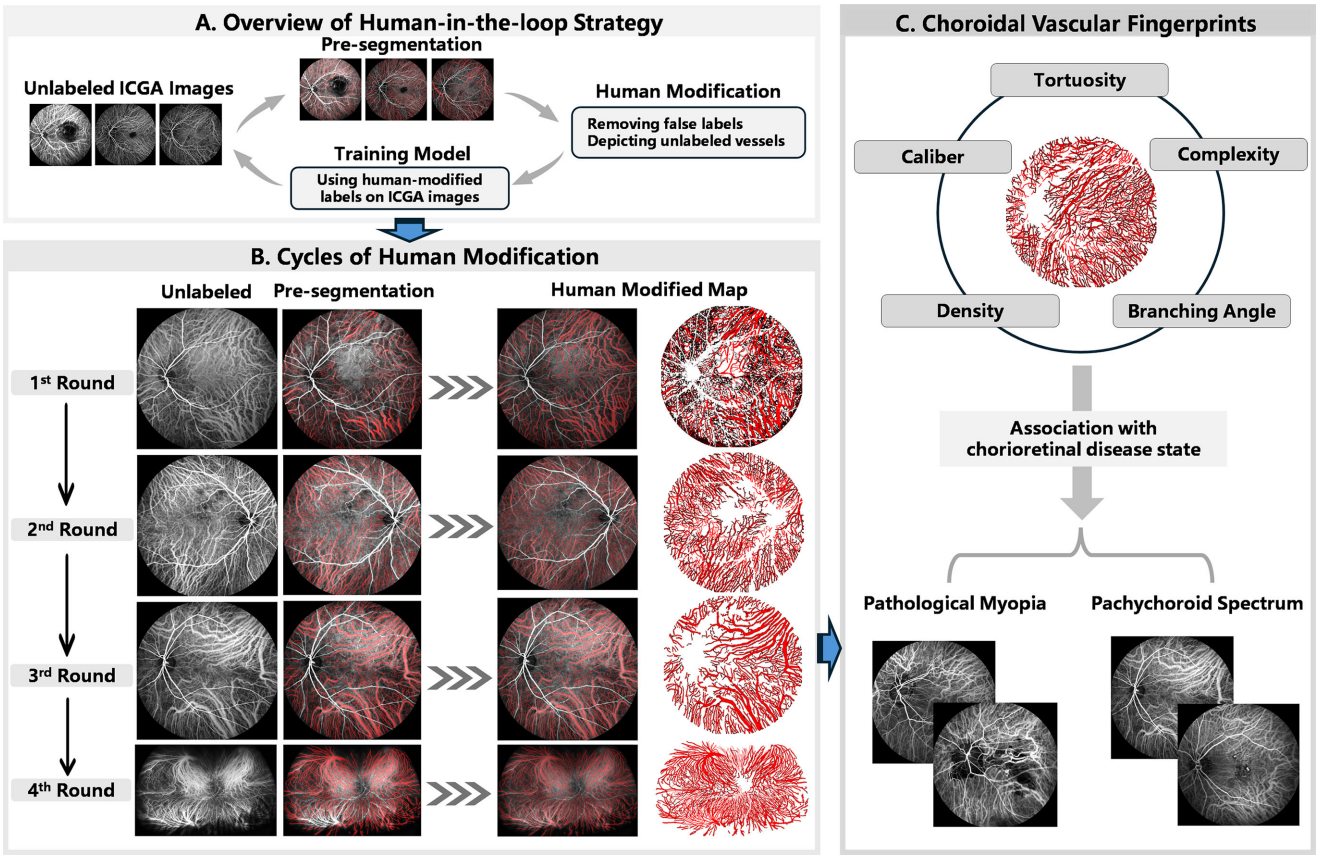

Figure 1. Flowchart of this study. **(A)** Overview of human-in-the-loop strategy: A pretrained generative adversarial network (GAN)-based model was applied for vessel presegmentation on ICGA images. These presegmentations were randomly selected and modified by human experts. The modified choroidal vascular maps were then used to fine-tune the pretrained model to segment choroidal vessels on ICGA images. This refined segmentation model was deployed on new unlabeled ICGA images to obtain an upgraded version of choroidal vascular segmentation. **(B)** Cycles of human modification: The iterative process was performed for three cycles on 55° view ICGA images and one cycle on UWF-ICGA images, progressively enhancing the model's ability to segment visible vessels. Examples of the presegmentation and human-modified segmentations for each cycle are presented in this section. **(C)** Choroidal vascular fingerprints: Quantification of caliber, complexity, tortuosity, branching angle, and density constitutes choroidal vascular fingerprints. The association between choroidal vascular fingerprints and chorioretinal diseases was evaluated.

were trained with a batch size of 4 and a learning rate of 0.0002.

Evaluation of Segmentation Performance

The iterative process of the HITL strategy ended once human experts (R.C. and Z.Z.) visually confirmed that the model could successfully segment visible choroidal vasculature (as defined in Supplementary Fig. S2: Vessel Annotation Protocol—Step 1 and Step 2) in test set. Then, the objective evaluation metrics at the pixel level were calculated in the final cycle to complement human assessment and reduce potential bias, including F1-score, the area under the receiver operating characteristic curve (AUC), accuracy, sensitivity, and specificity, between predictions of model and human modified choroidal vascular segmentations. To ensure the reliability of the evaluation results, the calculation of quantitative metrics conducted by another researcher (D.S.) was entirely independent of the annotation process.

Choroidal Vascular Fingerprints

The Retina-based Microvascular Health Assessment System pipeline was used to quantify vessel characteristics from the predicted choroidal vessel maps across five dimensions: density, complexity, tortuosity, caliber, and branching angle.[13,21] These parameters formed choroidal vascular fingerprints. Because the vascular trees were segmented into numerous vessel segments for analysis, resulting in hundreds of individual measurements per image for each metric, we used summary statistics, including mean, standard deviation, maximum, and minimum values to consolidate these measurements and provide a comprehensive overview of each image. These summary statistics offer a multifaceted representation of the measurements.[22,23] Supplementary Table S1 offers a detailed explanation of extracted choroidal vascular parameters.

Reliability of Choroidal Vascular Fingerprints

The intraclass correlation coefficients (ICC) were calculated for evaluating the intra-visit repeatability of all enrolled choroidal vascular measurements. Because ICGA is a dynamic process, changes in choroidal vascular fluorescence over time during ICGA imaging can inherently lead to measurement variability in choroidal vessels. Therefore, to minimize the impact of time and changes in patients' eye positions on the measurements, early-phase ICGA images

Investigative Ophthalmology & Visual Science

captured with a time interval of less than 10 seconds and under consistent eye positioning were selected for ICC calculation. A total of 39 eyes from 39 patients were included, with two images per eye. ICC values of <0.5, 0.5–0.75, 0.75–0.90, and ≥0.90 indicate poor, moderate, good, and excellent reliability, respectively.[24]

Association Between Choroidal Vascular Fingerprints and Chorioretinal Disease State

To evaluate the clinical significance of these choroidal vascular fingerprints on segmented choroidal vascular maps, we compared these parameters between normal controls (without any abnormalities on ICGA images) and those with pachychoroid spectrum diseases (CSC, PCV) and choroidal thinning disease (PM). We retrospectively included ICGA images from 394 patients with complete ICGA reports and definitive diagnoses, comprising 151 images from normal controls, 46 images from CSC patients, 130 images from PCV patients, and 67 images from PM patients. The median age of the participants was 50.03 (±19.43) years, and 235 (59.64%) were male. Primary normal ranges were established based on the current dataset.

Statistical Analysis

Continuous variables are reported as mean ± SD, whereas categorical variables are presented as frequencies and percentages. Extreme outliers for choroidal vascular parameters were removed using the Robustbase package in R software (range = 3), which accounts for skewness. To enable uniform comparison across variables and eliminate scale differences, we normalized the values of choroidal vascular parameters to SD units. Multivariable logistic regression models were used to examine the association between choroidal vascular parameters and CSC, PCV, and PM, with adjustments for age and sex.

For establishing normal ranges for each choroidal vascular measurement, outliers were initially removed through the interquartile range method. Normality for each variable was subsequently assessed using the Shapiro-Wilk test. For normally distributed data, the mean and standard deviation were computed to establish the 95% confidence interval (CI). For non-normally distributed data, the first and third quartiles were utilized as the bounds.

Given the multiple parameters and resulting multiple comparisons, *P* values were adjusted for the false discovery rate to control for type I error, with the significance level set at a two-tailed *P* value of 0.05. All statistical analyses were performed using R software (4.3.3)

Results

A total of four HITL cycles were performed to fine-tune the pre-trained model for choroidal vascular segmentation on 55° view ICGA images and UWF-ICGA images, with three cycles for 55° view ICGA images (50 images per cycle) and one cycle for UWF-ICGA images (20 images per cycle) (Fig. 1B). Detailed characteristics of images used in each cycle are summarized in the Table.

The average time needed to manually correct a pre-segmented 55° ICGA image decreased significantly with each cycle. For 55° ICGA pre-segmentations, the average time (mean±standard deviation) required for manual correction was 20.05 ± 2.15 minutes each for the first round, 5.40 ± 1.87 minutes each for the second round, and 1.38 ± 1.03 minutes each for the third round. For UWF-ICGA pre-segmentations, the human expert (R.C.) only needed to add a few missing vessel annotations in the peripheral area since the model could successfully identify choroidal vascular in the posterior area after training with the first three rounds of the HITL process. Thus the average time required for manual correction was just 10.49 ± 1.95 minutes per UWF-ICGA image. In comparison, manually segmenting choroidal vascular networks from scratch required approximately 50.23 ± 4.27 minutes per 55° ICGA image and 74.93 ± 5.82 minutes per UWF-ICGA image, highlighting that the HITL strategy significantly reduced the time required for training.

Accuracy of Choroidal Vessel Segmentation

The inter-grader Dice coefficient (R.C. and Z.Z.) was 0.870. The predicted choroidal vascular maps showed strong alignment with the ground truth: AUC = 0.975 (95% CI, 0.967–0.983), F1-score = 0.867 (95% CI, 0.856–0.878), accuracy = 0.950 (95% CI, 0.946–0.954), sensitivity = 0.858 (95% CI, 0.844–0.872), specificity = 0.972 (95% CI, 0.968–0.976). The model also demonstrated high accuracy in segmenting choroidal vasculature on UWF-ICGA images: AUC = 0.937 (95% CI, 0.914–0.960), F1-score = 0.780 (95% CI, 0.763–0.797), accuracy = 0.895 (95% CI, 0.862–0.928), sensitivity = 0.784 (95% CI, 0.762–0.806), specificity = 0.927 (95% CI, 0.895–0.959). Examples of predicted choroidal vessel networks on ICGA and UWF-ICGA images are shown in Figures 2 and 3.

Association Between Choroidal Vascular Fingerprints and Chorioretinal Diseases

The Retina-based Microvascular Health Assessment System extracted 164 choroidal vessel measurements from the

Table. Detailed Characteristics of ICGA Images Used in Each HITL Round

Tasks	Total	Normal	CSC	PCV	PM	AMD	Others
Model development (images)							
Round 1	50 (100%)	6 (12%)	9 (18%)	11 (22%)	7 (14%)	6 (12%)	11 (20%)
Round 2	50 (100%)	6 (12%)	7 (14%)	10 (20%)	9 (18%)	8 (16%)	10 (20%)
Round 3	50 (100%)	5 (10%)	10 (20%)	7 (14%)	15 (30%)	5 (10%)	8 (16%)
Round 4	20 (100%)	3 (15%)	1 (5%)	1 (5%)	0 (0%)	4 (20%)	11 (55%)
Association analysis							
Patients	394 (100%)	151 (38%)	46 (12%)	130 (33%)	67 (17%)		

AMD; age-related macular degeneration; CSC; central serous chorioretinopathy, PCV; polypoidal choroidal vasculopathy, PM; pathological myopia.

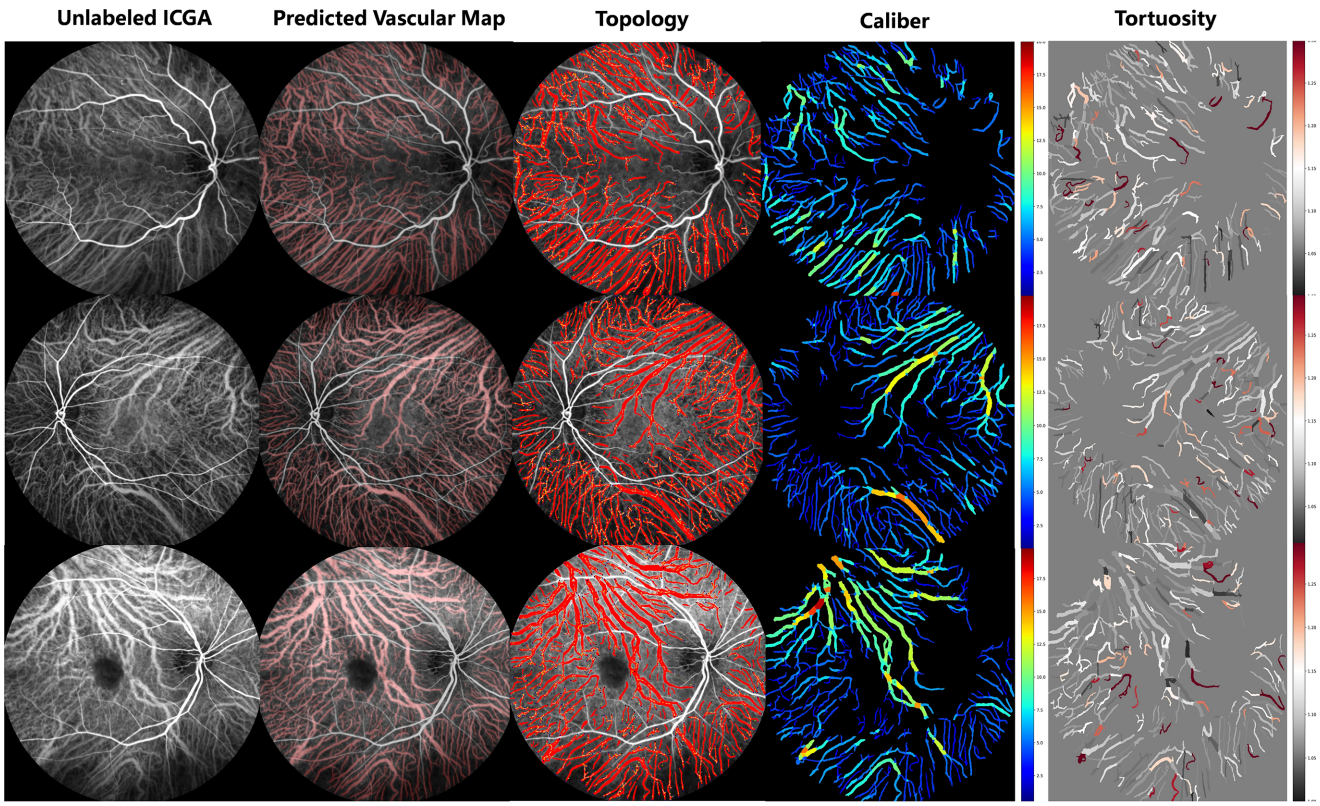

Figure 2. Examples of predicted choroidal vascular networks on ICGA images and vascular measurement plots.

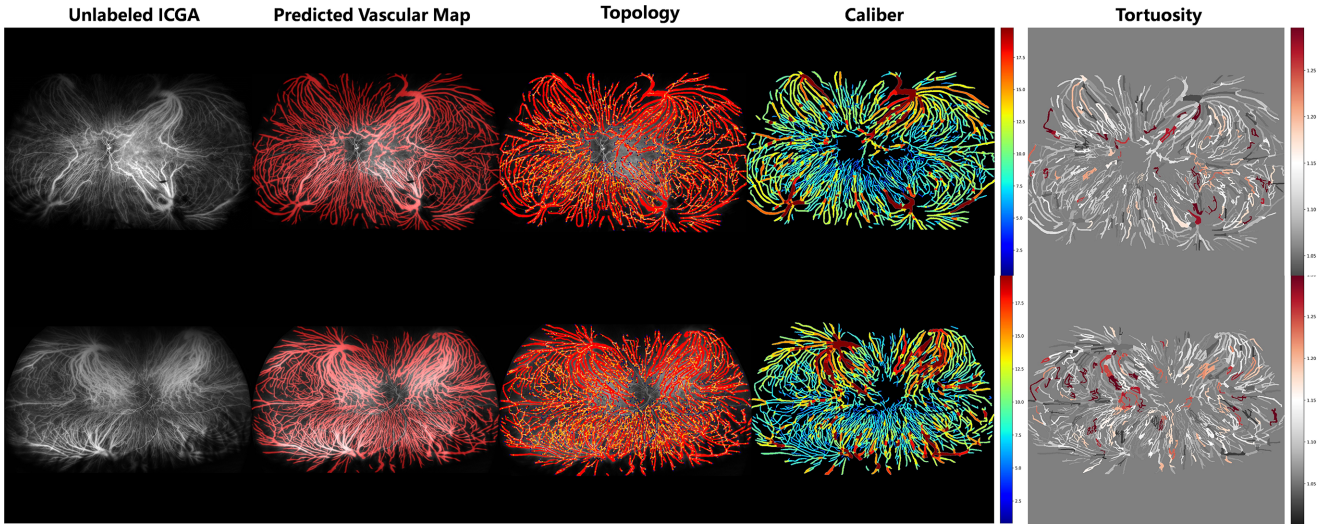

Figure 3. Examples of predicted choroidal vascular networks on UWF-ICGA images and vascular measurement plots.

predicted choroidal vessel segmentation, covering five categories: density, complexity, tortuosity, caliber and branching angle. After removing measurements with 90% missing data or where more than 95% of elements were the same value, 74 choroidal vessel measurements were included in further analysis. The ICC values ranged from 0.71 (95% CI, 0.51–0.84) to 0.97 (95% CI, 0.95–0.99). Details of ICC values in each measurement are provided in Supplementary Table S5. The significant associations (false discovery rate–adjusted $P < 0.05$) between various chorioretinal diseases and multiple vessel measurements are illustrated in Figure 4. Normal ranges of each choroidal vessel measurement are presented in Supplementary Table S6. All the results were adjusted for sex and age. Unadjusted results are shown in Supplementary Tables S2–S4.

The relationship between various choroidal vessel measurements and CSC is shown in Figure 4A. Twenty-six parameters were significantly associated with CSC after

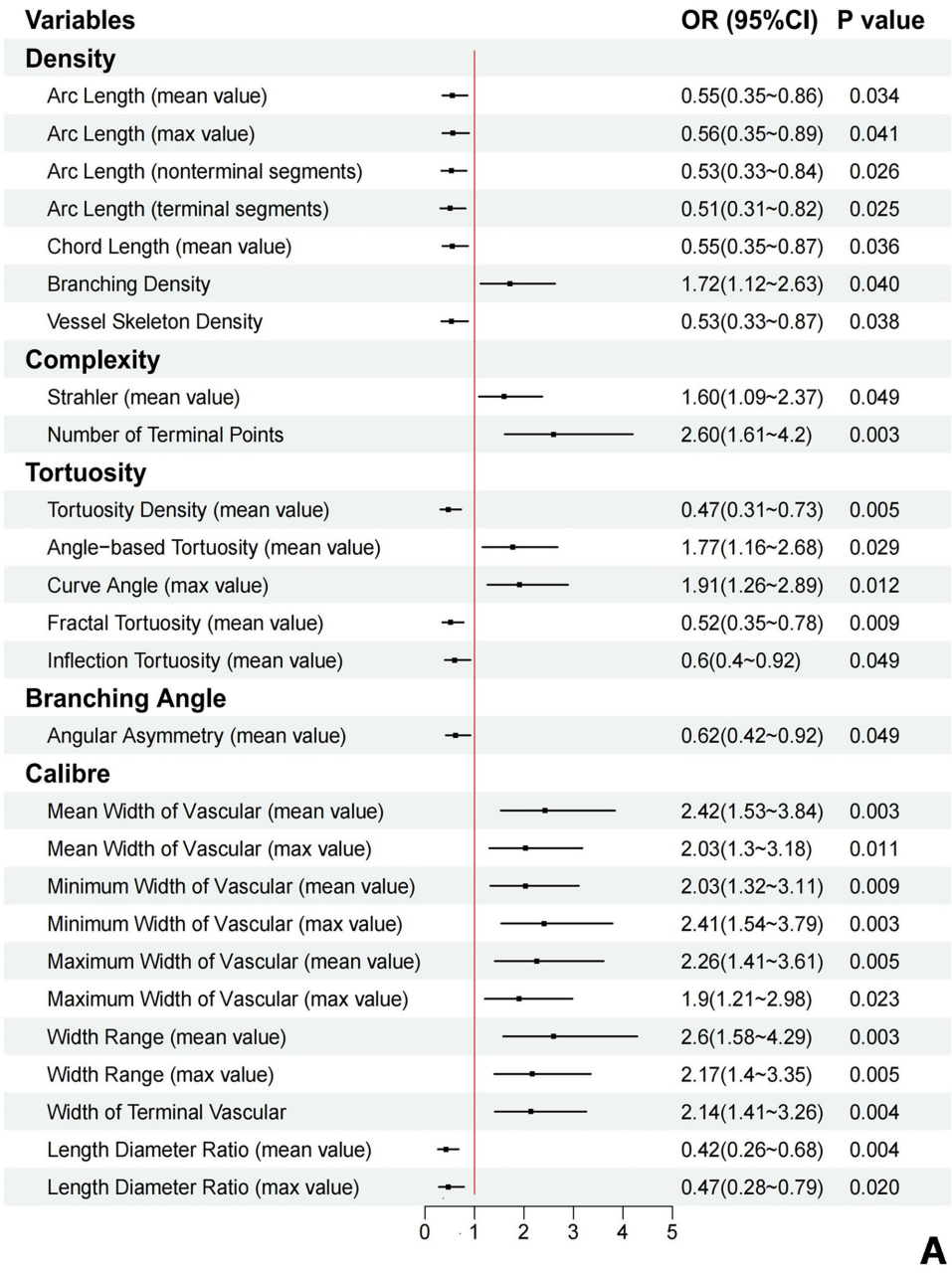

Figure 4. Association between chorioretinal diseases and selected choroidal vascular-related parameters. **(A)** Central serous chorioretinopathy. **(B)** Polypoidal choroidal vasculopathy. **(C)** Pathological myopia. *P* values were adjusted for sex and age.

adjusting for sex and age. The complexity-related parameters (Strahler number), most of the caliber-related parameters (mean caliber, minimum caliber, maximum caliber, caliber range, and terminal caliber), and tortuosity-related parameters (angle-based tortuosity, curve angle) were significantly and positively associated with CSC. In contrast, most of the choroidal vascular density-related parameters (arc length, chord length, and vessel skeleton density), tortuosity-related parameters (tortuosity density, fractal tortuosity, and inflection tortuosity), and all the branching angle-related parameters (angular asymmetry) were negatively correlated with CSC. Specifically, branching density (mean value per image) was associated with increased risk of CSC (odds ratio [OR] = 1.72 [95% CI, 1.12–2.63]), angle-based tortuosity (mean value per image) was also related to increased risk of CSC (OR = 1.77 [95% CI, 1.16–2.68]. Additionally, the mean width of the choroidal vascular (mean value per image) was associated with increased risk of CSC (OR = 2.24 [95% CI, 1.53–3.84]), the maximum width of choroidal vasculature (mean value per image) was associated with increased risk of CSC (OR = 2.26 [95% CI, 1.41–3.61]).

The association between multiple choroidal vessel parameters and PCV is shown in Figure 4B. Twenty-eight parameters were significantly associated with PCV after adjusting for sex and age. Among these, most complexity-related metrics (Strahler number, level, and number of terminal points), caliber-related metrics (mean caliber, maximum

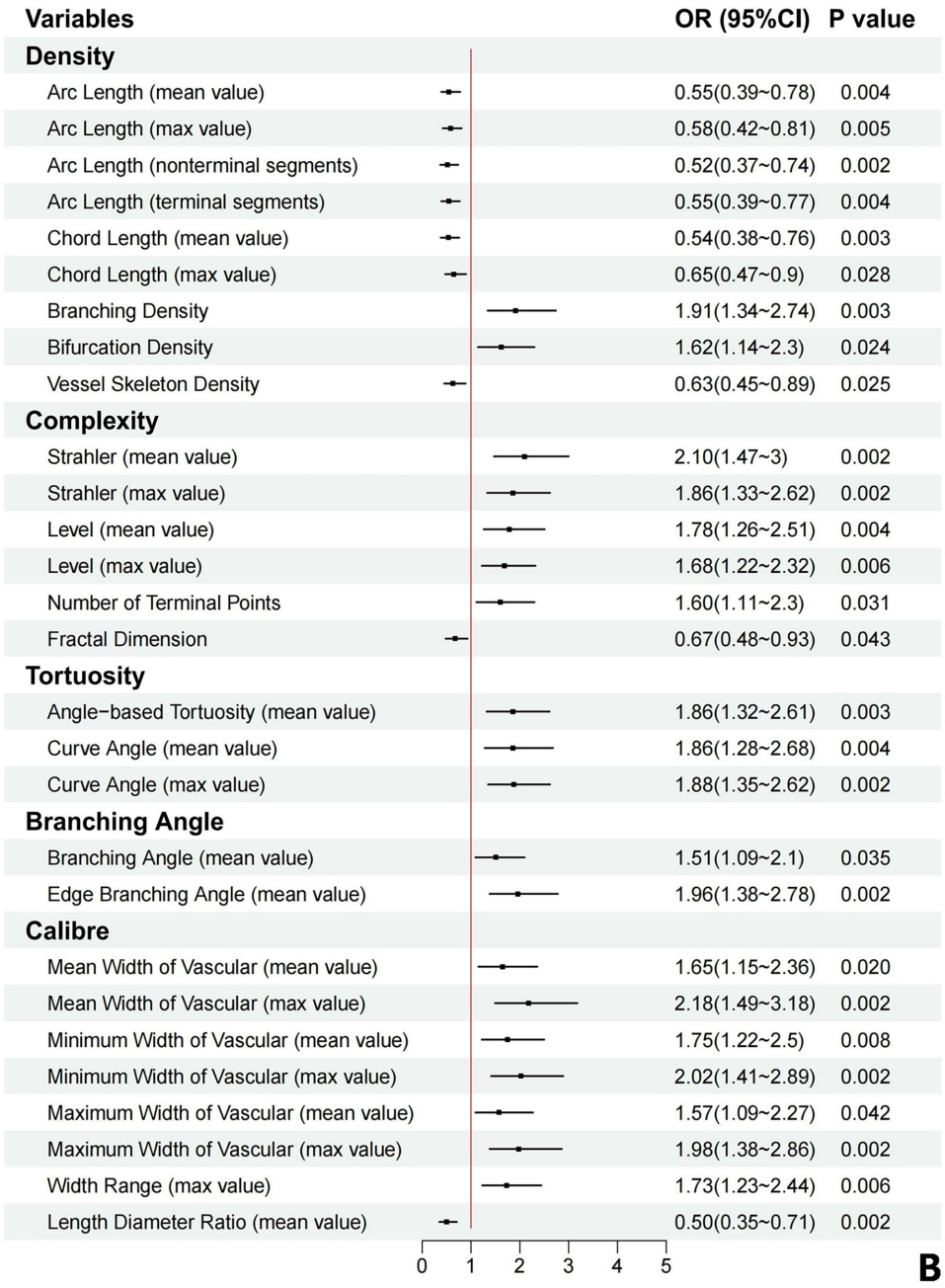

Figure 4. Continued.

caliber, minimum caliber, and caliber range), branching angle-related metrics (branching angle) and all tortuosity-related metrics were associated with increased risk of PCV. In contrast, most choroidal vascular density-related parameters (arc length, chord length, and vessel skeleton density) were inversely correlated with PCV. Specifically, branching density (mean value per image) was associated with increased risk of PCV (OR = 1.91 [95% CI, 1.34–2.74]), complexity-related metrics, Strahler number (mean value per image) was associated with increased risk of PCV (OR = 2.10 [95% CI, 1.43–3.00]), angle-based tortuosity (mean value per image) was associated with increased risk of PCV (OR = 1.86 [95% CI, 1.32–2.61]. Additionally, mean width of the choroidal vascular (mean value per image) was associated with increased risk of PCV (OR] = 1.65 [95% CI, 1.15–2.36]), maximum width of choroidal vasculature (mean value per image) was associated with increased risk of PCV (OR = 1.57 [95% CI, 1.09–2.27]).

The significant relationships between multiple choroidal vessel parameters and PM are illustrated in Figure 4C. Twenty-nine parameters were significantly associated with PM after adjusting for age and sex. Among these, density-related parameters (arc length and chord length), complexity-related parameters (Strahler number, level, and fractal dimension), caliber-related parameters (mean caliber, maximum caliber, minimum caliber, surface area, caliber range, and length diameter ratio) and branching angle-related parameters (Asymmetry Ratio) were positively corre-

Investigative Ophthalmology & Visual Science

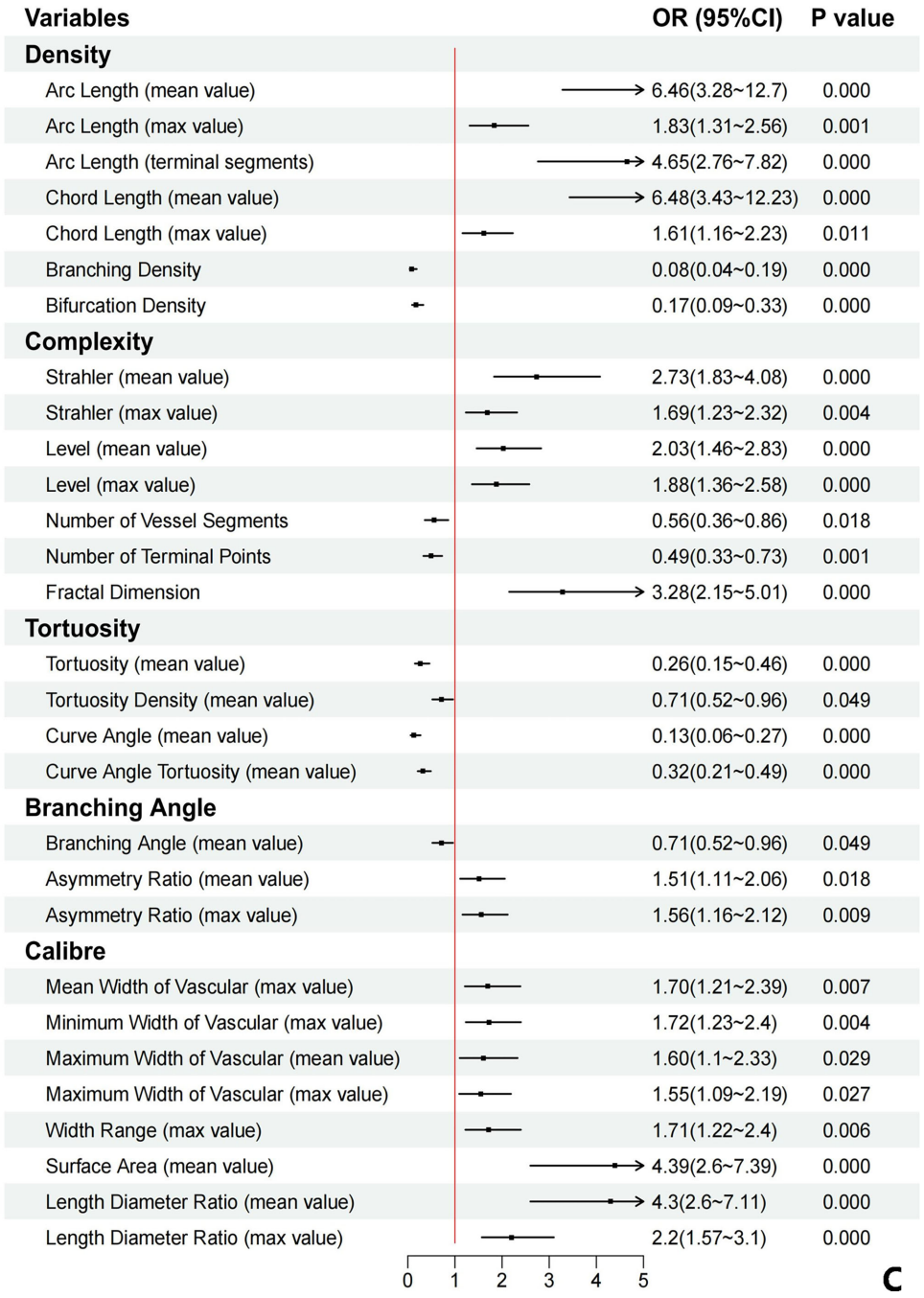

Figure 4. Continued.

lated with the occurrence of PM. On the contrary, most of the tortuosity-related parameters (tortuosity, tortuosity density, curve angle, curve angle tortuosity and inflection tortuosity) were negatively correlated with PM. Arc length (mean value per image) was associated with increased risk of PM (OR = 6.46 [95% CI, 3.28–12.70]), Strahler number (mean value per image) was associated with increased risk of PM (OR = 2.73 [95% CI, 1.84–4.08]), fractal dimension (mean value per image) was associated with increased risk of PM (OR = 3.28 [95% CI: 2.15–5.01]), asymmetry ratio (mean value per image) was associated with increased risk of PM (OR = 1.51 [95% CI, 1.11–2.06]). Besides, the mean width of choroidal vascular (max value per image) was also positively correlated to PM (OR = 1.70 [95% CI, 1.21–2.39])

Discussion

In this study, we developed an innovative high-precision choroidal vessel segmentation model using a HITL framework, significantly reducing labor requirements. This model demonstrated robust accuracy for both 55° view ICGA and UWF-ICGA images. Additionally, the algorithm automatically quantifies multidimensional choroidal vascular characteristics, namely choroidal vascular fingerprints. Our key findings indicated that choroidal vascular fingerprints can serve as

Investigative Ophthalmology & Visual Science

reliable and comprehensive biomarkers, significantly associated with CSC, PCV and PM. These quantified vascular features are expected to enhance our understanding of the different pathological processes of chorioretinal diseases.

Recent studies have increasingly focused on the relationship between choroidal vascular alterations and various chorioretinal diseases. Optical coherence tomography (OCT) can capture choroidal vascular-related biomarkers within macular regions, such as choroidal vascularity index on B-scan images, flow voids, and choroidal capillary density on OCT enface images.[25–27] However, the limited scanning area and potential artifacts may compromise the comprehensiveness and accuracy of these measurements. Our automatic segmentation model enabled effective quantification of vascular characteristics on 55° view ICGA and UWF-ICGA images, including density, complexity, tortuosity, branching angle, and caliber. This pioneering algorithm represents a promising approach for multidimensional analysis of complex choroidal vascular networks and objective evaluation of choroidal circulation in multiple diseases. The current study serves as an initial exploration using a retrospective dataset. Future research with larger sample sizes is needed to establish robust thresholds for choroidal vascular fingerprints, which may have greater clinical impact.

Choroidal venous overload is a key feature in CSC pathogenesis, with significant implications for treatment and prognosis.[28] Enlarged choroidal vessels and choroidal intervortex veins have been frequently observed on ICGA images of CSC patients.[29,30] Similarly, PCV is another phenotype of the pachychoroid disease spectrum, characterized by dilated choroidal veins and remodeling of choroidal vessels.[31,32] The current study provides a more detailed perspective for understanding various chorioretinal diseases. Most parameters related to caliber, complexity, and tortuosity were significantly associated with an increased risk of CSC and PCV. Moreover, PM eyes exhibited larger choroidal vascular diameters, possibly due to increased visibility of large choroidal vessels resulting from axial elongation-associated choriocapillaris loss.[33,34] These novel biomarkers are expected to become valuable additions to existing diagnostic criteria and to facilitate personalized management of multiple chorioretinopathies. A future longitudinal study is essential to monitor changes in choroidal fingerprints during the treatment of different diseases and to assess their potential utility in predicting clinical outcomes.

A well-developed image processing model requires massive training data with accurate annotation. However, labeling large-scale samples is labor-intensive and time-consuming. The HITL strategy encourages algorithms to interact with experienced specialists, assisting in improving both model performance and annotation efficiency in various tasks.[35] In the present study, the pretrained model initially segmented portions of the choroidal vascular network, significantly reducing the time required for human labeling compared to manual segmentation from scratch. Throughout the HITL strategy, the time required for manual correction decreased as the model's performance steadily improved with each round of HITL training, resulting in more accurate pre-segmentations in the next round and fewer corrections by the human expert. These findings demonstrate that the HITL strategy significantly reduced the time needed for training compared to the standard training procedure. However, the fact that both annotators refined the same presegmentation generated by the model may introduce bias when assessing inter-expert variability. Besides, although objective metrics validated the model's final performance, the HITL cycles in this study were stopped based on human visual impressions. Incorporating objective performance thresholds to guide HITL termination might be beneficial in future exploration.

This study has some limitations. First, the study used an in-house ICGA image dataset, with all participants from the Chinese region. Large-scale ICGA databases covering multiethnic populations and a wide range of diseases are needed to evaluate the generalizability of our algorithm and to establish widely applicable thresholds for each measurement. Additionally, the definition of "normal control" in this study was limited to individuals without significant choroidal vascular abnormalities. Future research should aim to address issues related to potential population variation in the normal values of choroidal vascular fingerprints. Third, ICGA is an invasive procedure, and future investigations on noninvasive imaging modalities, such as OCT enface images of various retinal and choroidal layers, and noninvasive ICGA-like choroidal vessel quantification are promising using generative artificial intelligence.[36,37]

In summary, the current study represents the first attempt to reveal choroidal vascular fingerprints. The proposed algorithm can quantify choroidal vascular features from multiple perspectives, with significant associations to CSC, PCV, and PM. These findings underscore the potential of applying choroidal vascular fingerprints for accurate and comprehensive analysis of choroidal vascular abnormalities, shedding light on the exploration of the pathological mechanisms behind them.

Acknowledgments

The authors thank the InnoHK HKSAR Government for providing valuable supports.

Supported by the Start-up Fund for RAPs under the Strategic Hiring Scheme (P0048623) from HKSAR, Global STEM Professorship Scheme (P0046113), and Henry G. Leong Endowed Professorship in Elderly Vision Health. The sponsors or funding organizations had no role in the design or conduct of this research.

Conflicts of Interest: M.H. and D.S. are inventors of the technology mentioned in the study patented as "A retinal chorioretinal vessel segmentation method based on the conditional generative adversarial network (CN114782339A)".

Data and Code Availability: The data used for model development of this study are not openly available due to reasons of privacy. The authors do not have the permission to distribute the dataset publicly. The code for the segmentation model architecture is available at: https://github.com/NVIDIA/pix2pixHD. The quantification code used in our study is part of a pending patent application (CN114782339A) and cannot be released at this stage.

Disclosure: **R. Chen**, None; **Z. Zhao**, None; **M. Yusufu**, None; **X. Shang**, None; **M. He**, CN114782339A (P); **D. Shi**, CN114782339A (P)

References

1. Nickla DL, Wallman J. The multifunctional choroid. *Prog Retin Eye Res*. 2010;29:144–168.
2. He G, Zhang X, Gan Y, et al. Choroidal vein alterations in pachychoroid disease with choroidal vascular hyperperme-

ability: evaluated by wide-field indocyanine green angiography. *Invest Ophthalmol Vis Sci*. 2023;64(11):25.
3. Cheung CMG, Lee WK, Koizumi H, Dansingani K, Lai TYY, Freund KB. Pachychoroid disease. *Eye (London)*. 2019;33:14–33.
4. Jonas JB, Jonas RA, Bikbov MM, Wang YX, Panda-Jonas S. Myopia: histology, clinical features, and potential implications for the etiology of axial elongation. *Prog Retin Eye Res*. 2023;96:101156.
5. Cui Y, Zhu Y, Lu ES, et al. Widefield swept-source OCT angiography metrics associated with the development of diabetic vitreous hemorrhage: a prospective study. *Ophthalmology*. 2021;128:1312–1324.
6. Stanga PE, Lim JI, Hamilton P. Indocyanine green angiography in chorioretinal diseases: indications and interpretation: an evidence-based update. *Ophthalmology*. 2003;110:15–21; quiz 2–3.
7. Verma A, Maram J, Alagorie AR, et al. Peripheral extent of the choroidal circulation by ultra-widefield indocyanine green angiography in healthy eyes. *Br J Ophthalmol*. 2021;105:824–828.
8. Baek J, Lee JH, Jung BJ, Kook L, Lee WK. Morphologic features of large choroidal vessel layer: age-related macular degeneration, polypoidal choroidal vasculopathy, and central serous chorioretinopathy. *Graefes Arch Clin Exp Ophthalmol*. 2018;256:2309–2317.
9. Lee A, Ra H, Baek J. Choroidal vascular densities of macular disease on ultra-widefield indocyanine green angiography. *Graefes Arch Clin Exp Ophthalmol*. 2020;258:1921–1929.
10. Jeong A, Lim J, Sagong M. Choroidal vascular abnormalities by ultra-widefield indocyanine green angiography in polypoidal choroidal vasculopathy. *Invest Ophthalmol Vis Sci*. 2021;62(2):29.
11. Hirahara S, Yasukawa T, Kominami A, Nozaki M, Ogura Y. Densitometry of choroidal vessels in eyes with and without central serous chorioretinopathy by wide-field indocyanine green angiography. *Am J Ophthalmol*. 2016;166:103–111.
12. Mookiah MRK, Hogg S, MacGillivray TJ, et al. A review of machine learning methods for retinal blood vessel segmentation and artery/vein classification. *Med Image Anal*. 2021;68:101905.
13. Shi D, Lin Z, Wang W, et al. A deep learning system for fully automated retinal vessel measurement in high throughput image analysis. *Front Cardiovasc Med*. 2022;9:823436.
14. Wan S, Hou Y, Bao F, et al. Human-in-the-loop low-shot learning. *IEEE Trans Neural Netw Learn Syst*. 2021;32:3287–3292.
15. Ambale-Venkatesh B, Lima JAC. Human-in-the-loop artificial intelligence in cardiac MRI. *Radiology*. 2022;305:80–81.
16. Wang J, Guo B, Chen LJA. Human-in-the-loop machine learning: a macro-micro perspective. *arXiv*. Preprint posted online February 21, 2022, doi:abs/2202.10564.
17. Mosqueira-Rey E, Hernández-Pereira E, Alonso-Ríos D, Bobes-Bascarán J, Fernández-Leal Á. Human-in-the-loop machine learning: a state of the art. *Artif Intell Rev*. 2022;56:3005–3054.
18. Madono K, Nakano T, Kobayashi T, Ogawa TJA-PS, Summit I. Efficient human-in-the-loop object detection using bi-directional deep SORT and annotation-free segment identification. In: *2020 Asia-Pacific Signal and Information Processing Association Annual Summit and Conference (APSIPA ASC)*. Piscataway, NJ: IEEE, 2020:1226–1233.
19. Zhang R, Torabi F, Guan L, Ballard DH, Stone P. Leveraging human guidance for deep reinforcement learning tasks. *arXiv*. Preprint posted online September 21, 2019, doi:1909.09906.
20. Shi D, Zhou Y, He S, et al. Cross-modality labeling enables noninvasive capillary quantification as a sensitive biomarker for assessing cardiovascular risk. *Ophthalmol Sci*. 2024;4(3):100441.
21. Yusufu M, Friedman DS, Kang M, et al. Retinal vascular fingerprints predict incident stroke: findings from the UK Biobank cohort study. *Heart*. 2025;111:306–313.
22. Huang Y, Li C, Shi D, et al. Integrating oculomics with genomics reveals imaging biomarkers for preventive and personalized prediction of arterial aneurysms. *EPMA J*. 2023;14:73–86.
23. Yusufu M, Chen Y, Dayimu A, et al. Retinal vascular measurements and mortality risk: evidence from the UK Biobank Study. *Transl Vis Sci Technol*. 2024;13(1):2.
24. Koo TK, Li MY. A guideline of selecting and reporting intraclass correlation coefficients for reliability research. *J Chiropr Med*. 2016;15:155–163.
25. Lin F, Zhao Z, Li F, et al. Longitudinal macular retinal and choroidal microvasculature changes in high myopia. *Invest Ophthalmol Vis Sci*. 2021;62(15):1.
26. Qiu B, Zhang X, Li Z, et al. Characterization of choroidal morphology and vasculature in the phenotype of pachychoroid diseases by swept-source OCT and OCTA. *J Clin Med*. 2022;11:3243.
27. Rochepeau C, Kodjikian L, Garcia MA, et al. Optical coherence tomography angiography quantitative assessment of choriocapillaris blood flow in central serous chorioretinopathy. *Am J Ophthalmol*. 2018;194:26–34.
28. van Rijssen TJ, van Dijk EHC, Yzer S, et al. Central serous chorioretinopathy: towards an evidence-based treatment guideline. *Prog Retin Eye Res*. 2019;73:100770.
29. Pauleikhoff LJB, Diederen RMH, Chang-Wolf JM, et al. Choroidal vascular changes on ultrawidefield indocyanine green angiography in central serous chorioretinopathy: CERTAIN Study Report 1. *Ophthalmol Retina*. 2024;8:254–263.
30. Spaide RF, Gemmy Cheung CM, Matsumoto H, et al. Venous overload choroidopathy: A hypothetical framework for central serous chorioretinopathy and allied disorders. *Prog Retin Eye Res*. 2022;86:100973.
31. Ruamviboonsuk P, Lai TYY, Chen SJ, et al. Polypoidal choroidal vasculopathy: updates on risk factors, diagnosis, and treatments. *Asia Pac J Ophthalmol*. 2023;12:184–95.
32. Cheung CMG, Wong MYZ, Teo KYC. Choroidal vascular alterations in age-related macular degeneration and polypoidal choroidal vasculopathy. *Retina*. 2023;43:1–7.
33. Su L, Ji YS, Tong N, et al. Quantitative assessment of the retinal microvasculature and choriocapillaris in myopic patients using swept-source optical coherence tomography angiography. *Graefes Arch Clin Exp Ophthalmol*. 2020;258:1173–1180.
34. Al-Sheikh M, Phasukkijwatana N, Dolz-Marco R, et al. Quantitative OCT angiography of the retinal microvasculature and the choriocapillaris in myopic eyes. *Invest Ophthalmol Vis Sci*. 2017;58:2063–2069.
35. Holzinger A, Plass M, Kickmeier-Rust MD, et al. Interactive machine learning: experimental evidence for the human in the algorithmic loop. *Appl Intell*. 2018;49:2401–2414.
36. Shi D, Zhang W, He S, et al. Translation of color fundus photography into fluorescein angiography using deep learning for enhanced diabetic retinopathy screening. *Ophthalmol Sci*. 2023;3(4):100401.
37. Chen R, Zhang W, Song F, et al. Translating color fundus photography to indocyanine green angiography using deep-learning for age-related macular degeneration screening. *NPJ Digit Med*. 2024;7:34.

Investigative Ophthalmology & Visual Science